Journal of Oceanology and Limnology
Vol. 42, No. 2, pp. 511-521, 2024
https://doi.org/10.1007/s00343-023-2401-5

Research Paper

Different responses of two adjacent artificial beaches to Typhoon Hato in Zhuhai, China*

Jun ZHU[1, 2], Qing WANG[1, **], Chao ZHAN[1], Fengjuan SUN[1], Wenhao HUA[1], Jianhui LIU[2], Hongshuai QI[2], Yu YANG[1]

[1] *Coastal Research Institute, Ludong University, Yantai 264025, China*
[2] *Third Institute of Oceanography, Ministry of Natural Resources, Xiamen 261005, China*

Received Dec. 27, 2022; accepted in principle Mar. 3, 2023; accepted for publication Apr. 12, 2023

Abstract Major differences in beach erosion between two neighboring artificial beaches Xiangluwan Beach (XL beach) and Meiliwan Beach (ML beach) in Zhuhai, China, were studied after Super Typhoon Hato. In this study, a fully nonlinear Boussinesq wave model (FUNWAVE)-Total Variation Diminishing (TVD) was used to distinguish the main impact factors, their relative contributions, and the hydrodynamic mechanisms underlying the different beach responses. Results show that compared to the ML beach, the main reason for the relatively weak erosion on Xiangluwan (XL) beach was the smaller beach berm height (accounting for approximately 75.9% of the erosion response). Regarding the beach with a higher berm, the stronger wave-induced undertow flow, along with the higher sediment concentration, led to a higher offshore sediment transport flux, resulting in more severe erosion relative to the beach with a smaller berm height. The second most important reason explaining the weak erosion on XL beach was the absence of seawalls (accounting for approximately 17.9% of the erosion response). Wave reflection induced by the seawall could cause higher suspended sediment concentration, resulting in a toe scouring near the seawall. The offshore submerged breakwater protected XL beach slightly (accounting for approximately 6.1% of the erosion response). Due to the higher water level induced by storm surge, most of the wave energy could penetrate through the submerged breakwater. The effect of the larger berm width of XL beach was negligible. Compared to the beach with a larger berm width, the erosion/deposition regions in the beach with a narrower berm width showed shoreward migration, without significant changes in the erosion/deposition extent. Despite of this, the larger berm width could reduce the wave energy reaching the shoreline. This study of the storm stability of artificial beaches may be applied to beach restoration design.

Keyword: beach erosion; berm height; berm width; seawall; fully nonlinear Boussinesq wave model (FUNWAVE)

1 INTRODUCTION

Artificial beaches are an effective way against ongoing beach erosion (Liu et al., 2020). With the gradual increase in the number of artificial beaches, the issue of artificial beach stability, especially during storms, has increasingly become a research hotspot (Zhu et al., 2022). Similar to natural beaches, artificial beaches protect the coast by adapting themselves to a super-dynamic environment. Many scholars have studied the beach response from different perspectives, such as upper beach erosion (Brenner et al., 2018), berm narrowing (Roberts et al., 2013), shoreline retreating (Pang et al., 2021), sandbar migrating (Li et al., 2022), sediment coarsening (Ma et al., 2019; Zeng et al., 2021), and post-typhoon recovery (Ge et al., 2017).

There are many factors that affect beach

* Supported by the National Natural Science Foundation of China (Nos. 42006176, 42330406, U1706220, 41901006) and the Basic Research Project of the Science and Technology Innovation Development Program of in Yantai (No. 2022JCYJ028)
** Corresponding author: schingwang@126.com

responses to storms, which can be categorized into three aspects (Zhu et al., 2022). The first aspect involves storm characteristics, including the storm intensity, duration, and frequency (Dissanayake et al., 2015; Brenner et al., 2018). The second aspect entails beach characteristics, which reflect the beach adaptability, including the shoreline orientation (Loureiro et al., 2012), beach buffer width (Lee et al., 2011), beach berm height (Zhu et al., 2022), beach length (Burvingt et al., 2018), beach exposure level (Brooks et al., 2017), and sediment grain size (Scott et al., 2016). The third aspect involves the hydrodynamic characteristic parameters induced by the interaction among tides, waves and bathymetry (Qi et al., 2010; Feng et al., 2020), including incident wave angle (Zhu et al., 2019), wave nonlinearity (Zhang et al., 2021), and undertow flow (Xie et al., 2017). Of the three aspects, the second aspect is the most important influencing factor of the storm stability of artificial beaches because beach characteristics also constitute a major component of beach restoration design. Therefore, the study of the response of artificial beach characteristics to storms is important for beach restoration design.

Recently, Zhu et al. (2022) reproduced beach profile changes of two adjacent artificial beaches during storm landfall by using the FUNWAVE (fully nonlinear Boussinesq wave) model (Shi et al., 2012; Gao et al., 2021) and found that the beach berm height could significantly influence beach erosion processes. Their results suggested that a high berm could induce more offshore sediment transport and cause significant beach erosion relative to a beach with a lower berm. Although they already identified the main factor determining the coastal erosion differences between two neighboring beaches, Xiangluwan beach (XL beach) and Meiliwan beach (ML beach), in Zhuhai, there are secondary factors that should not be ignored, such as the beach berm width and the effects of seawalls and offshore submerged breakwater.

The present study is a continuation of that conducted by Zhu et al. (2022) and has two objectives. The first objective was to further confirm the effect of the beach berm height on the beach storm response, and the second objective was to quantify the contribution of all other factors inducing large differences in beach erosion.

2 STUDY AREA

Zhuhai is a coastal city located on the western coast of the Zhujiang (Pearl) River estuary, Guangdong Province, China (Fig.1a). At the end of 2016, Zhuhai completed two artificial beach restoration projects, namely, ML and XL beaches. XL beach is located approximately 3.6 km south of ML beach (Fig.1b), and both beaches are oriented eastward (Fig.1c & d, respectively). The lengths of XL and ML beaches were designed as 1.3 and 1.1 km, respectively.

Figure 2 shows the beach profiles of ML and XL beaches before the storm, which are aligned perpendicular to the shoreline for easy comparison. The mean sea water level (MSL), mean high water level of the spring tide (MHWS), and mean total water level (MTWL) during the storm landing period are also shown in the figure for reference. The two beaches have the same sediment grain size (0.5 mm), similar offshore seabed elevations (Fig. 2a) and beach face slopes, at approximately 1/10 (Fig. 2b). There are several differences between the two beaches. ML beach exhibits a berm height of 2.9 m relative to MSL (Fig.2a), while XL beach exhibits a berm height of only 2.1 m. The reason for the different designed beach berm heights is that the elevation of the road behind XL beach is much lower, at only 2.1 m. The berm width of ML beach is approximately 50 m, while that of XL beach is approximately 61 m. The backshore of XL beach directly connects to the road, while a seawall is built behind the backshore of ML beach. There occurs an old offshore submerged breakwater (its location is shown in Fig.1d) with a crest level of approximately -0.4 m and located 550 m from the XL coast (Fig.2a). The differences between ML and XL beaches are listed in Table 1.

On August 23, 2017, Super Typhoon Hato struck Zhuhai. The trajectory of Hato is shown in Fig.1a (tracking data were retrieved from the Chinese typhoon weather website (http://typhoon.weather.com.cn/)). This typhoon was one of the strongest typhoons to affect the region of the Zhujiang River Delta in southern China over the last several decades (Takagi et al., 2018; Hall et al., 2019). It broke historical records in terms of the storm surge height and area of flooding, with a maximum storm tide of 3.4 m and a maximum offshore wave height close to 4 m, as determined through numerical simulation of storm landfall (Chen et al., 2019). Although ML and XL beaches are adjacent beaches and their beach profile directions are similar and close to the main incident wave direction, the erosion extent notably differed between XL and ML

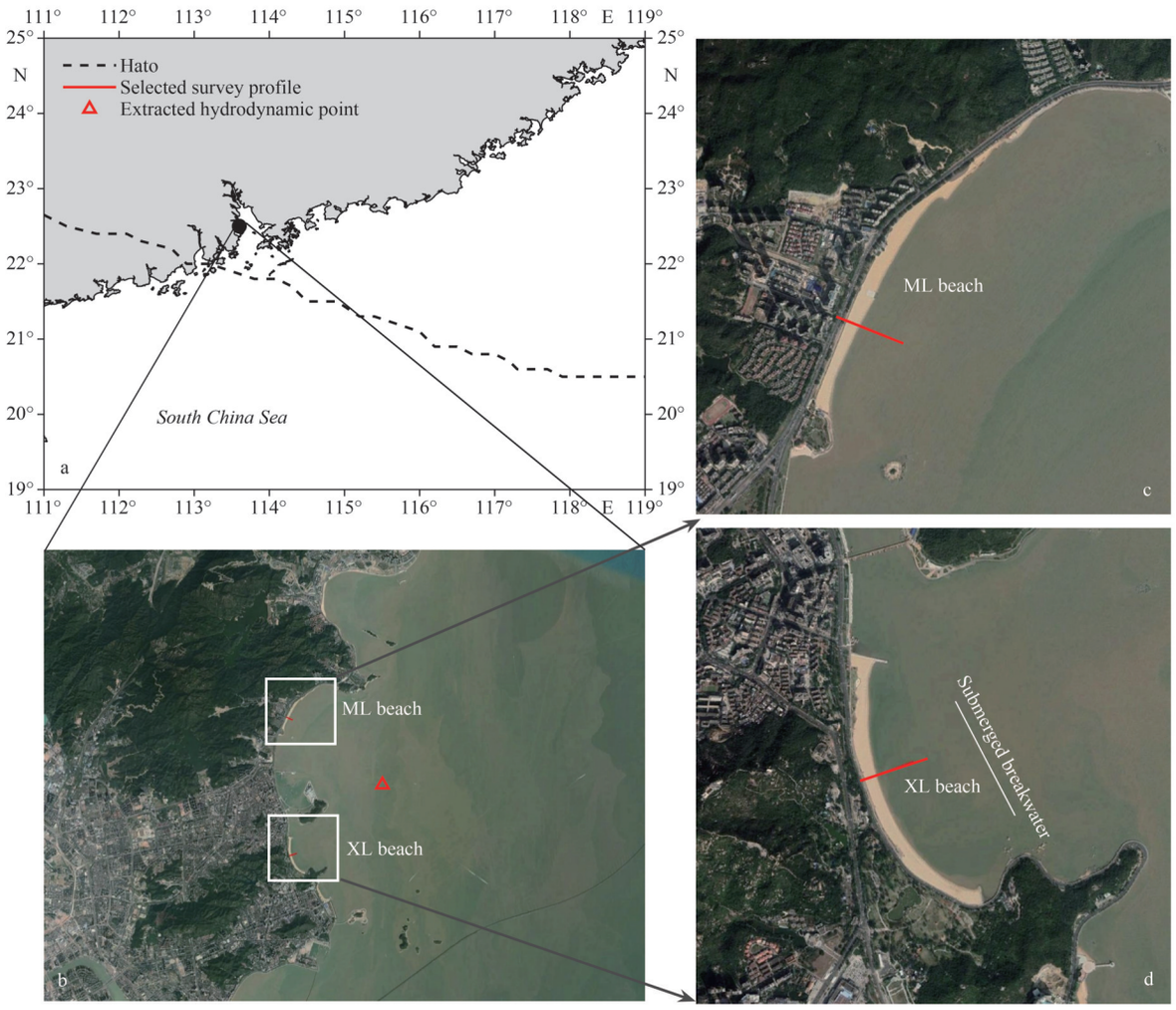

Fig.1 Study area (a & b) and detailed views of the ML beach (c) and XL beach (d) (modified from Zhu et al. (2022))

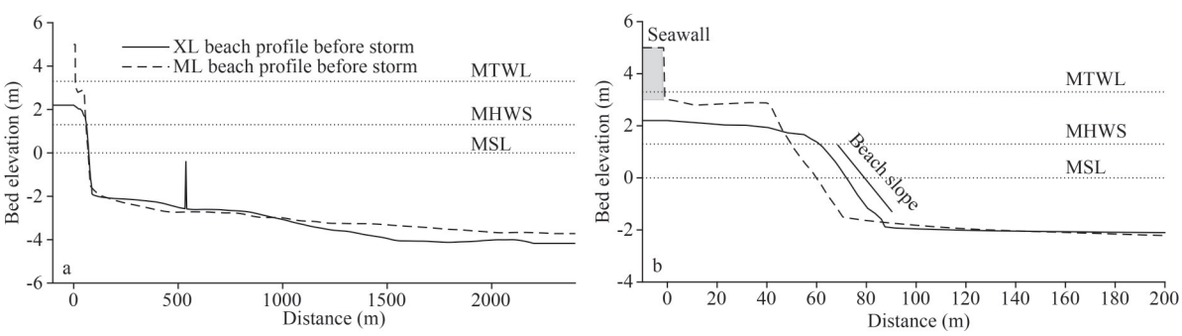

Fig.2 Beach profile before the storm (a) and magnified views (b) of XL and ML beaches

MSL: mean sea water level; MHWS: mean high water level of the spring tide; MSL: mean total water level. Modified from Zhu et al. (2022).

Table 1 Differences in the designs and beach responses of XL and ML beaches

Beach name	Offshore submerged breakwater	Berm height (m)	Berm width (m)	Presence of seawalls	Retreat (m)
XL beach	Yes	2.1	61	No	5
ML beach	No	2.9	50	Yes	17

beaches. The mean retreat of the berm edge at XL beach was approximately 5 m, while that at ML beach reached approximately 17 m. Figure 3 shows the beach profile changes before and after the storm.

3 RESEARCH METHOD

Of the methods to study the beach response to storms, numerical models are considered a very effective and convenient tool (Yin et al., 2019). In the present study, FUNWAVE-Total Variation Diminishing (TVD) (Shi et al., 2012) was used, which is a total variation diminishing version (Shi et al., 2016) of the fully nonlinear Boussinesq wave model. The suspended load and bedload sediment transport were implemented to address bed level change (Tehranirad et al., 2017). Recently, the roller/underflow effect has been considered in sediment transport processe (Zhu et al., 2022). Detailed documentation on the hydrodynamic and sediment transport models can be found in Shi et al. (2012) and Zhu et al. (2022), respectively.

3.1 Model setup

As shown in Fig. 1a, both XL and ML beaches are located to the right of the typhoon's movement path, and the azimuths of the two beaches differ by only 41°, with each beach profile offset by ±20.5° relative to the main wave direction at the wave extraction point (Fig.1b). It can be expected that this angular deviation will be further reduced as the waves propagate to the shoreline. Therefore, in this present study, a one-dimensional (1D) simulation was carried out, in which only the cross-shore sediment transport was considered, while the longshore sediment transport was not included.

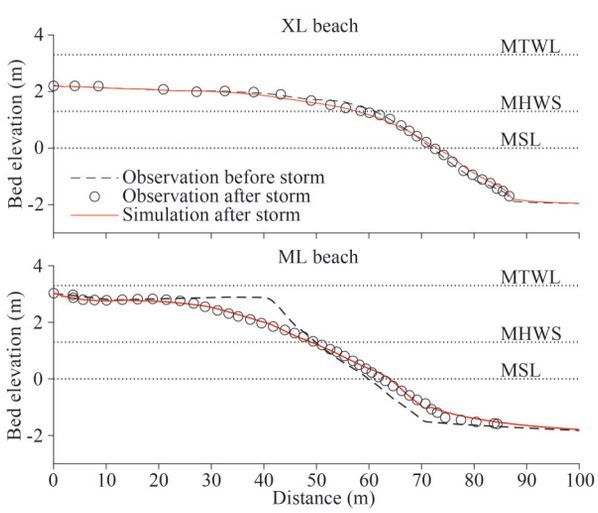

Fig.3 Comparisons of the simulated and observed beach profiles of XL (upper) and ML (lower) beaches

The bathymetries extracted from survey data for XL and ML beaches were measured on May 24, 2017, before the storm, and on August 25, right after the storm (Hato made landfall on August 23). Please note that the interval between the two bathymetry surveys was a little long, which may have an impact on model validation. However, as the finding of Liu et al. (2021), ML and XL beaches are low-energy coast, and the average value of $H_{1/10}$ throughout the year is 0.38 m. Under normal wave conditions, the profile changes of the two beaches should be small. Fortunately, there is no other storms passed during the interval of the two surveys. The offshore forcing, hourly incident significant wave height and total water level during storm crossing were extracted from the simulation results of Chen et al. (2019). The location of the hydrodynamic extraction point is shown in Fig.1b.

Based on the Courant-Friedrichs-Levy (CFL) numerical stability criterion, CFL=0.5 was used in the present study. A set of random waves were generated by using JONSWAP spectrum on the offshore side (Fig.2a). At both the onshore and offshore side boundaries, a sponge layer was specified to absorb the reflected waves. To prevent the offshore submerged breakwater from eroding in the model, a non-erodible layer was applied above the breakwater. The median grain size was set to 0.5 mm, which is consistent with observations of the two artificial beaches.

3.2 Model evaluation

Model evaluation was based on quantitative comparisons between the simulated and observed bed level changes (Fig. 3). We surveyed the profiles (Fig. 1c & d) of the two beaches before and after beach nourishment in May and August 2017, respectively. Regarding ML beach, a large amount of sediment was removed from the berm and dumped at the beach toe, while the adjacent XL beach exhibited limited erosion during the storm. In contrast to ML beach, the erosion magnitude at XL beach was 4–5 times smaller than that at ML beach. The root mean square (rms) difference for XL beach was only 7.8 cm and that for ML beach was approximately 12.0 cm.

Detailed model evaluation results, including the surface wave elevation, significant wave height, sediment concentration, and bed level change, can be found in Zhu et al. (2022).

3.3 Model scenario

Based on the satisfactory comparisons between the modeled and observed bed level changes, we used the model to further address why these adjacent beaches responded differently to the same typhoon and determined the contributions of each factor. In the present study, five scenarios were designed, as listed in Table 2. Case 1 is the prototype simulation of XL beach, and cases 2–5 are all hypothetical beaches that gradually approach the prototype beach of ML beach. In hypothetical case 2, the submerged breakwater was removed and smoothed considering the adjacent bathymetry. In hypothetical cases 3 and 4, the berm was smoothly elevated or lengthened to prevent any sudden changes in terrain.

4 RESULT AND DISCUSSION

4.1 Effect of the offshore submerged breakwater

Cases 1 and 2 were designed to distinguish the effect of the offshore submerged breakwater on the bed level changes during the storm. Bed level changes after the storm in cases 1 and 2 are shown in Fig.4. The beach profiles before the storm are also depicted in the figure for reference. As shown in this figure, a large amount of sediment was removed from the berm and dumped at the beach toe. However, the resulting bed levels after the storm in the cases with and without an offshore submerged breakwater were very similar, suggesting that the offshore submerged breakwater at XL beach could not protect it during the storm.

Zhuhai is characterized by a mean tidal range of 1.2 m (Liu et al., 2019), which is classified as a microtidal range according to the classification of Davies (1964). Under normal water level and wave conditions, the offshore submerged breakwater can effectively protect the beach by decreasing the incident wave energy because the breakwater crest level is -0.4 m relative to the MSL. During the storm landing period, the MTWL reached 3.3 m, while the mean significant wave height increased to 2.4 m (Zhu et al., 2022). With such a high storm surge, most of the wave energy could penetrate through the submerged breakwater. Figure 5 shows the snapshots of instantaneous wave propagation in the two cases. The beach profiles before the storm are also depicted in the figure for reference. In case 1, the significant wave height on the leeward side was approximately 98% of that on the windward side of the submerged breakwater, and notable wave reflection occurred in the windward sea. Given that the wave energies reaching the berms were so close

Table 2 Model scenarios

Case name	Submerged breakwater	Berm height (m)	Berm width (m)	Presence of seawalls	Description
Case 1	Yes	2.1	61	No	Prototype of XL beach
Case 2	No	2.1	61	No	Hypothetical beach
Case 3	No	2.9	61	No	Hypothetical beach
Case 4	No	2.9	50	No	Hypothetical beach
Case 5	No	2.9	50	Yes	Hypothetical beach but close to prototype of ML beach

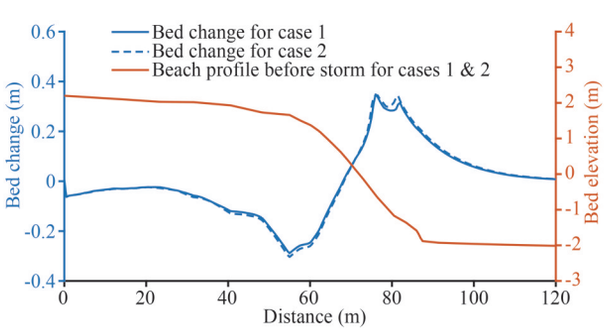

Fig.4 Changes of bed level after the storm, and beach profiles before the storm under the scenarios with (case 1) and without (case 2) the offshore submerged breakwater

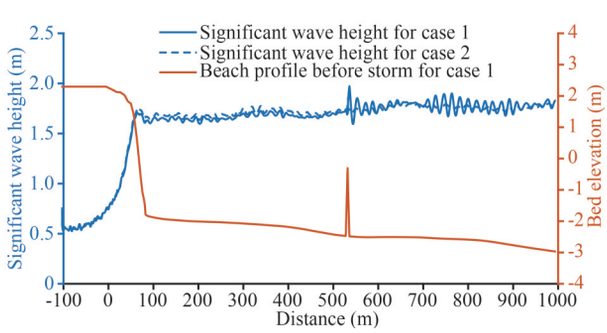

Fig.5 Changes of significant wave heights, and beach profiles before the storm under the scenario with (case 1) and without (case 2) the offshore submerged breakwater

in the cases with and without a submerged breakwater, there is no doubt that the bed changes in these two cases are similar (Fig.4).

4.2 Effect of the berm height

To quantify the impact of the berm height on the beach responses to the storm, we increased the berm height at XL beach from 2.1 m in case 2 to 2.9 m in case 3. The beach profiles before and after the storm and bed level changes in cases 2 and 3 are shown in Fig.6. After the storm, the beach profile with a larger berm height (case 3) showed much more severe erosion than that with a smaller berm height (case 2). The maximum scour depth increased from 0.3 m in case 2 to 0.5 m in case 3.

The different beach responses are related to the corresponding hydrodynamic conditions (Pang et al., 2021). Therefore, the distributions of the wave height across the beach berm were further compared between the two cases (Fig.7). As waves propagated to the coastline, the significant wave heights in the two cases were relatively similar until a clear difference in the position of the berm edge occurred (X=60 m). When the beach berm height was increased from cases 2 to 3, the significant wave height near the coastline decreased from 0.71 to 0.37 m, decreasing by approximately 47.8%, and the wave energy decreased by approximately 72.8%. The notable dissipation in wave energy was mainly used to transfer sediment seaward.

The difference in beach response between the two cases could be further explained by the sediment transport processes shown in Fig.8. The figure illustrates the snapshots of undertow flux Q_u, sediment concentration C, and sediment flux induced by the undertow Q_uC. There was no significant difference in the distribution of the undertow flux (Fig.8a) between the two cases, especially on the seaward side of the berm edge (X=60 m). This mainly occurred because the beach slope and the associated significant wave height in the two cases were identical. Notable differences in the undertow flux could be found over the beach berms, where the wave heights greatly differed between cases 2 and 3 (Fig.7). The sediment concentration on the higher berm (case 3) was much higher than that on the lower berm (case 3) with two peaks: one is located at the beach berm edge, and the other is located at the beach toe (Fig. 8b). Due to the higher sediment concentration on the higher berm, the sediment flux due to the undertow was generally higher (Fig.8c). Therefore, more sediment could be transported offshore in the higher berm case (case 3). This is the reason the higher berm case had more erosion/deposition.

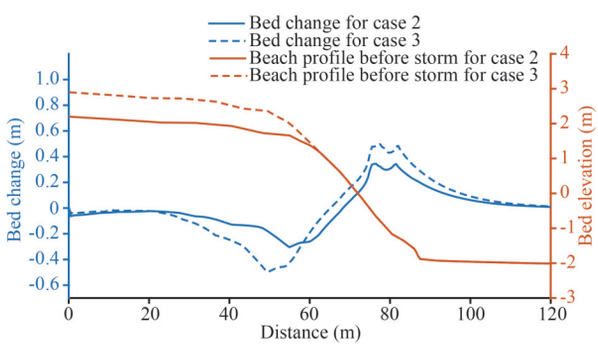

Fig.6 Same plot as Fig.4 but for the lower berm beach (case 2) and higher berm beach (case 3)

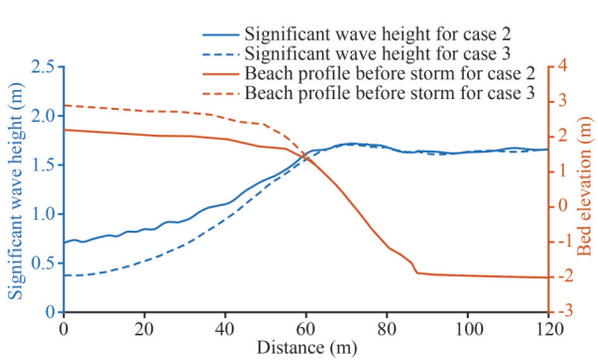

Fig.7 Same plot as Fig.5 but for the lower berm beach (case 2) and higher berm beach (case 3)

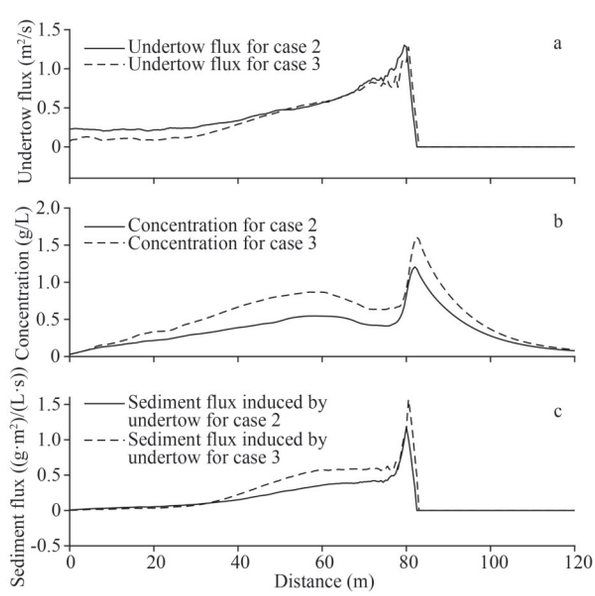

Fig.8 Changes in the undertow flux (a), suspended sediment concentration (b), and sediment flux induced by undertow (c) for the lower berm beach (case 2) and higher berm beach (case 3)

4.3 Effect of the beach berm width

As shown in Fig.2 and Table 1, XL and ML beaches differed in not only the beach berm height but also the beach berm width. The berm width at XL beach is approximately 61 m, while that at ML beach is approximately 50 m. To account for the influence of the beach berm width on the beach response to the storm, a smaller berm width scenario (case 4) was further simulated for a comparison to a larger berm width scenario (case 3) (Fig.9). Compared to those in case 3, the erosion/deposition regions in case 4 showed shoreward migration, and the notable parts of bed changes in the two cases had similar trends except for a shoreward translation in the horizontal direction. This suggests that the berm width probably exerts a non-significant influence on the beach response to storms.

The distributions of the significant wave height across the beach berm and beach face in cases 3 and 4 were compared and shown in Fig.10. When the beach berm width was narrowed from 61 to 50 m, the wave breaking zone experienced a landward movement of approximately 10 m, and the significant wave heights over the beach berm notably increased. Beaches with larger berm widths could not significantly reduce the loss of sand due to storms. Nonetheless, they could better protect the coast by reducing waves reaching the shoreline.

The undertow flux Q_u, suspended sediment concentration C, and sediment flux induced by undertow Q_uC for beaches with the larger berm width (case 3) and smaller berm width (case 4) were further compared in Fig.11. As the berm width decreases, the strong undertow zone is significantly narrowed (Fig. 11a). Compared with the wider berm beach (case 3), the two sediment concentration peaks for narrower berm beach (case 4) have a significant landward movement (Fig.11b). Due the shoreward translation of undertow and sediment concentration, the sediment flux due to undertow has a landward movement around at 13 m (Fig.11c), without obvious variation of erosion/deposition extent.

4.4 Effect of the seawall

The last difference between XL and ML beaches is the presence of a seawall behind the backshore of ML beach, while no seawall occurs at XL beach. To account for the effect of the seawall, a hypothetical beach with a seawall (case 5) was modeled and compared to case 4. With the construction of a seawall (case 5), the profile changes exhibited approximately the same general shape as those in the case without a seawall (case 4), except that a trench formed near the seawall (Fig.12). This is consistent with the findings of Ruggiero and McDougal (2001). A seawall is a shore-protection

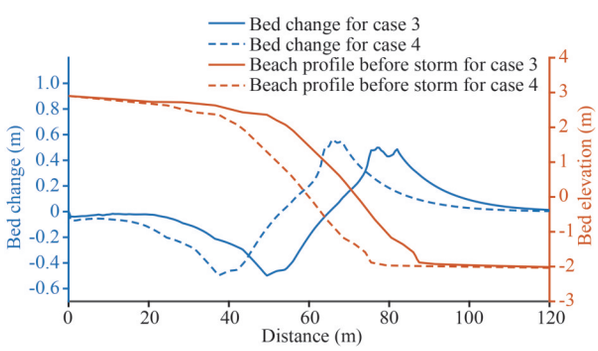

Fig.9 Same plot as Fig. 4 but for beaches with the larger berm width (case 3) and smaller berm width (case 4)

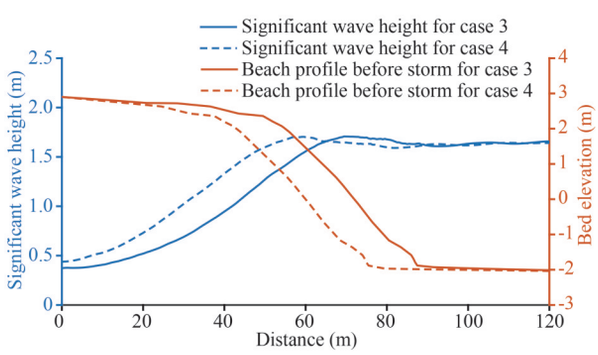

Fig.10 Same plot as Fig. 5 but for beaches with the larger berm width (case 3) and smaller berm width (case 4)

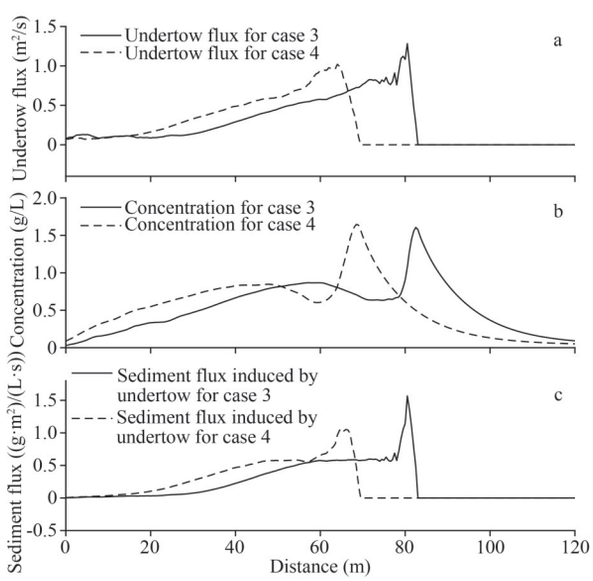

Fig.11 Same plot as Fig. 8, but for the larger berm width (case 3) and smaller berm width (case 4)

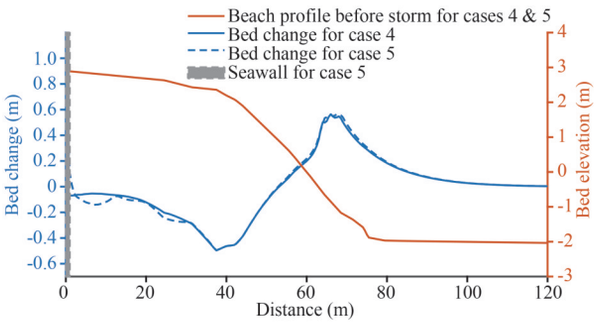

Fig.12 Same plot as Fig.4 but for beaches without (case 4) and with (case 5) a seawall behind the beach backshore

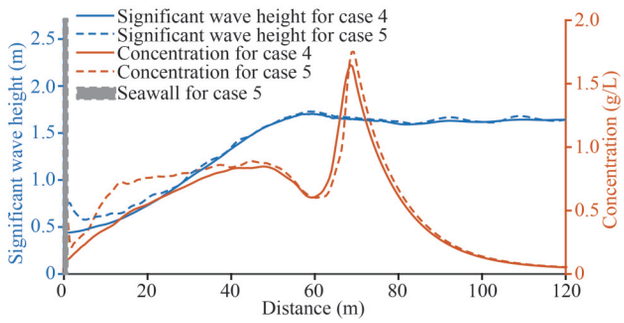

Fig.13 Changes in significant wave heights, and suspended sediment concentration under the scenarios without (case 4) and with (case 5) a seawall behind the beach backshore

structure but not a beach-protection structure. Wave reflection induced by seawalls is the main cause of toe scour (McDougal et al., 1996).

The distributions of the significant wave height and the suspended sediment concentration across the beach berm and beach face in cases 4 and 5 were further compared, as shown in Fig.13. With reflection due to the seawall, the mean significant wave height near the seawall increased significantly. Although a considerable part of the wave energy was reflected (approximately 43.5%), most of the reflected energy dissipated on the beach berm near the seawall, resulting in a higher suspended sediment concentration over beach berm. Under the influence of offshore undertow flow, a trench formed near the seawall.

4.5 Relative contributions of each impact factor

The previous subsections detail the morphology changes and relevant hydrodynamic mechanisms. This section further examines the relative contributions of each impact factor, including the berm height, berm width, the presence of the offshore submerged breakwater, and the absence of seawalls behind the backshore.

The erosion volumes per unit width for all scenarios are listed in Table 3, and their relative contributions are listed in Table 4. The beach erosion per unit width caused by Typhoon Hato at XL beach was approximately 8.23 m^3/m. The offshore breakwater provided little protection for the beach, as it only reduced the erosion at XL beach by 0.29 m^3/m. The smaller berm height was the major impact factor leading to weak erosion at XL beach, which reduced beach erosion by approximately 3.58 m^3/m. Compared to that of ML beach, XL beach has a larger berm width, which further reduced beach erosion by approximately 0.02 m^3/m. Finally, beach erosion was further reduced by 0.83 m^3/m due to the absence of seawalls behind the beach.

During the same storm, the response of XL beach was much weaker than that of the neighboring ML

Table 3 Erosion volume per unit width under all scenarios

Case name	Description	Erosion volume (m^3/m)
Case 1	Prototype of XL beach	8.23
Case 2	=case 1, but without an offshore submerged breakwater	8.52
Case 3	=case 2, but with a larger berm height	12.10
Case 4	=case 3, but with a smaller berm width	12.12
Case 5	=case 4, but with seawalls	12.95

Table 4 Relative contributions of each impact factor

Item	Submerged breakwater	Berm height	Berm width	Seawall
	Case 2–case 1	Case 3–case 2	Case 4–case 3	Case 5–case 4
Changes in the erosion volume per unit width (m^3/m)	0.29	3.58	0.02	0.83
Contribution (%)	6.1	75.9	0.4	17.9

beach. The main impact factor was the small berm height at XL beach (accounting for approximately 75.9% of the erosion response) (Table 4). To quantify the impact of the berm height on coast erosion during storms, Zhu et al. (2022) defined a berm height parameter $\gamma=(h_{\text{berm}}-\text{MTWL})/H_{\text{sig}}$, where h_{berm} is the berm height, MTWL is the still water level during storm landing, and H_{sig} is the offshore significant wave height. Zhu et al. (2022) demonstrated that the erosion efficiency, i.e., the eroded volume per unit width normalized by H_{sig}^2, increases with the berm height parameter, and the increase declines as the berm height approaches the MTWL. The berm height parameter γ values of XL and ML beaches were -0.65 and -0.22, respectively, resulting in significantly different erosion efficiencies of 1.0 and 3.2 for XL and ML beaches, respectively.

The second most important impact factor was the absence of seawalls, which accounted for approximately 17.9% of the erosion response (Table 4). Although the seawall exerted a limited impact on the entire beach profile during storms, wave reflection induced by seawalls is the main mechanism causing scour troughs near seawalls. Estimating the maximum scour depth near seawalls has thus far been a very challenging undertaking.

The contribution of the offshore submerged breakwater is relatively small, accounting for approximately 6.1% of the erosion response. However, this does not suggest that the offshore submerged breakwater is useless. The breakwater plays an important role in protecting the beach under normal water level and wave conditions.

The last important impact factor is the wide beach width, which accounted for only 0.4% of the erosion response. There exists almost no relationship between the erosion volume and the beach berm width during storms when the amount of sand is sufficient. Despite this finding, beaches with larger berm widths could better protect the coast by reducing waves reaching the shoreline. In addition, the relationship between the erosion volume and the beach berm width when the amount of sand is insufficient deserves further study because it is important to determine minimum beach berm width during beach nourishment design.

5 CONCLUSION

A fully nonlinear Boussinesq wave model, FUNWAVE-TVD, was used to simulate the beach response to Typhoon Hato, which imposed substantial but different effects on erosion at two neighboring artificial beaches, XL and ML beaches. The observations showed that ML beach was eroded much more severely than XL beach. Compared to ML beach, XL beach contains an offshore submerged breakwater, smaller berm height, and larger berm width, and there is no seawall located in the backshore area. To quantify the relative contributions of each impact factor, four additional hypothetical cases were modeled based on the prototype of XL beach.

The berm height, in fact, could significantly influence beach erosion during storms. The relatively smaller beach berm height was the main reason for the weak erosion at XL beach (accounting for approximately 75.9% of the erosion response). The second most important reason was the absence of seawalls (accounting for approximately 17.9% of the erosion response). The offshore submerged breakwater provided less protection for the beach during storms (accounting for approximately 6.1% of the erosion response). There exists almost no relationship between the erosion volume per unit width and the beach berm width during the storm when the amount of sand is sufficient.

Since artificial beach characteristics greatly influence the storm response, we should design beaches in a reasonable way. The beach berm height should be reasonably selected based on local storm dynamics and conditions. Seawalls behind the beach backshore with upright forms should be avoided to reduce wave reflection. The construction of offshore submerged breakwaters cannot protect the beach during storm landing due to storm surge, but protection under normal hydrodynamic conditions remains sufficient. Although a larger beach berm width exerts the smallest impact on the beach response to storms, it reduces the wave energy reaching the shoreline. The selection of the beach width should consider the need for coastal protection and recreational space.

6 DATA AVAILABILITY STATEMENT

The datasets generated during the current study are available from the corresponding author upon reasonable request.

7 ACKNOWLEDGMENT

We thank Dr. Fengyan SHI of the University of Delaware for his guidance on the use of the FUNWAVE model and appreciate the help received

from Dr. Wenping GONG of Sun Yat-sen University, who graciously shared the large-domain simulation results of storm waves and tides.

References

Brenner O T, Lentz E E, Hapke C J et al. 2018. Characterizing storm response and recovery using the beach change envelope: fire Island, New York. *Geomorphology*, **300**: 189-202, https://doi.org/10.1016/j.geomorph.2017.08.004.

Brooks S M, Spencer T, Christie E K. 2017. Storm impacts and shoreline recovery: mechanisms and controls in the southern North Sea. *Geomorphology*, **283**: 48-60, https://doi.org/10.1016/j.geomorph.2017.01.007.

Burvingt O, Masselink G, Scott T et al. 2018. Climate forcing of regionally-coherent extreme storm impact and recovery on embayed beaches. *Marine Geology*, **401**: 112-128, https://doi.org/10.1016/j.margeo.2018.04.004.

Chen Y R, Chen L H, Zhang H et al. 2019. Effects of wave-current interaction on the Pearl River Estuary during Typhoon Hato. *Estuarine*, *Coastal and Shelf Science*, **228**: 106364, https://doi.org/10.1016/j.ecss.2019.106364.

Davies J L. 1964. A morphogenic approach to world shorelines. *Zeitschrift für Geomorphologie*, **8**(5): 127-142, https://doi.org/10.1127/zfg/mortensen/8/1964/127.

Dissanayake P, Brown J, Wisse P et al. 2015. Effects of storm clustering on beach/dune evolution. *Marine Geology*, **370**: 63-75, https://doi.org/10.101/jmargeo.2015.10.010.

Feng X, Dong B X, Ma G F et al. 2020. Topographic and hydrodynamic influence on rip currents and alongshore currents on headland beaches in China. *Journal of Coastal Research*, **95**: 468, https://doi.org/10.2112/si95-091.1.

Gao J L, Ma X Z, Dong G H et al. 2021. Investigation on the effects of Bragg reflection on harbor oscillations. *Coastal Engineering*, **170**: 103977, https://doi.org/10.1016/j.coastaleng.2021.103977.

Ge Z P, Dai Z J, Pang W H et al. 2017. LIDAR-based detection of the post-typhoon recovery of a meso-macro-tidal beach in the Beibu Gulf, China. *Marine Geology*, **391**: 127-143, https://doi.org/10.1016/j.margeo.2017.08.008.

Hall B J, Xiong Y X, Yip P S Y et al. 2019. The association between disaster exposure and media use on post-traumatic stress disorder following Typhoon Hato in Macao, China. *European Journal of Psychotraumatology*, **10**(1): 1558709, https://doi.org/10.1080/20008198.2018.1558709.

Lee F C, Hsu J R C, Lin W H. 2011. Appraisal of storm beach buffer width for cyclonic waves. *Coastal Engineering*, **58**(11): 1049-1061, https://doi.org/10.1016/j.coastaleng.2011.06.005.

Li Y, Zhang C, Chen S B et al. 2022. Influence of artificial sandbar on nonlinear wave transformation: experimental investigation and parameterizations. *Ocean Engineering*, **257**: 111540, https://doi.org/10.1016/.oceaneng.2022.111540.

Liu G, Cai F, Qi H S et al. 2019. Morphodynamic evolution and adaptability of nourished beaches. *Journal of Coastal Research*, **35**(4): 737-750, https://doi.org/10.2112/jcoastres-d-18-00037.1.

Liu G, Cai F, Qi H S et al. 2020. A summary of beach nourishment in China: the past decade of practices. *Shore & Beach*, **88**(3): 65-73, https://doi.org/10.34237/1008836.

Liu G, Qi H S, Cai F et al. 2021. Morphodynamic evolution of post-nourishment beach scarps in low-energy and micro-tidal environment. *Journal of Marine Science and Engineering*, **9**(3): 303, https://doiorg/10.3390/jmse9030303.

Loureiro C, Ferreira Ó, Cooper J A G. 2012. Extreme erosion on high-energy embayed beaches: Influence of megarips and storm grouping. *Geomorphology*, **139-140**: 155-171, https://doi.org/10.1016/i.geomorph.2011.10.013.

Ma B B, Dai Z J, Pang W H et al. 2019. Dramatic typhoon-induced variability in the grain size characteristics of sediments at a meso-macrotidal beach. *Continental Shelf Research*, **191**: 104006, https://doi.org/10.1016/jcsr.2019.104006.

McDougal W G, Kraus N C, Ajiwibowo H. 1996. The effects of seawalls on the beach: part II, numerical modeling of SUPERTANK seawall tests. *Journal of Coastal Research*, **12**(3): 702-713, https://doi.org/10.2307/4298518.

Pang W H, Ge Z P, Dai Z J et al. 2021. The behaviour of beach elevation contours in response to different wave energy environments. *Earth Surface Processes and Landforms*, **46**(2): 443-454, https://doi.org/10.1002/esp.5036.

Qi H S, Cai F, Lei G et al. 2010. The response of three main beach types to tropical storms in South China. *Marine Geology*, **275**(1-4): 244-254, https://doi.org/10.1016/jmargeo.2010.06.005.

Roberts T M, Wang P, Puleo J A. 2013. Storm-driven cyclic beach morphodynamics of a mixed sand and gravel beach along the Mid-Atlantic Coast, USA. *Marine Geology*, **346**: 403-421, https://doi.org/10.1016/j.margeo.2013.08.001.

Ruggiero P, McDougal W G. 2001. An analytic model for the prediction of wave setup, longshore currents and sediment transport on beaches with seawalls. *Coastal Engineering*, **43**(3-4): 161-182, https://doi.org/10.1016/s0378-3839(01)00012-6.

Scott T, Masselink G, O'Hare T et al. 2016. The extreme **2013**/2014 winter storms: beach recovery along the southwest coast of England. *Marine Geology*, **382**: 224-241, https://doi.org/10.1016/i.margeo.2016.10.011.

Shi F, Kirby J T, Tehranirad B et al. 2016. FUNWAVE-TVD, Documentation and User's Manual (Version 3.0). Research Report No. CACR-11-03, https://doi.org/10.21079/11681/45641.

Shi F Y, Kirby J T, Harris J C et al. 2012. A high-order adaptive time-stepping TVD solver for Boussinesq modeling of breaking waves and coastal inundation. *Ocean Modelling*, **43-44**: 36-51, https://doi.org/10.1016/j.ocemod.2011.12.004.

Takagi H, Xiong Y, Furukawa F. 2018. Track analysis and storm surge investigation of 2017 Typhoon Hato: were the warning signals issued in Macau and Hong Kong timed appropriately? *Georisk*, **12**(4): 297-307, https://doi.org/10.1080/17499518.2018.1465573.

Tehranirad B, Kirby J T, Shi F Y et al. 2017. Does a morphological adjustment during tsunami inundation increase levels of hazard? *Tsunamis*, https://doi.org/10.1061/9780784480311.015.

Xie M X, Zhang C, Yang Z W et al. 2017. Numerical modeling of the undertow structure and sandbar migration in the surfzone. *China Ocean Engineering*, **31**(5): 549-558, https://doi.org/10.1007/s13344-017-0063-9.

Yin K, Xu S D, Huang W R et al. 2019. Modeling beach profile changes by typhoon impacts at Xiamen coast. *Natural Hazards*, **95**(3): 783-804, https://doi.org/10.1007/s11069-018-3520-8.

Zeng L, Zhan C, Wang Q et al. 2021. Sediment coarsening in tidal flats and stable coastline of the abandoned southern yellow river sub-delta in response to fluvial sediment flux decrease during the past decades. *Frontiers in Marine Science*, **8**: 761368, https://doi.org/10.3389/fmars.2021.761368.

Zhang C, Li Y, Cai Y et al. 2021. Parameterization of nearshore wave breaker index. *Coastal Engineering*, **168**: 103914, https://doi.org/10.1016/j.coastaleng.2021.103914.

Zhu J, Cai F, Shi F Y et al. 2019. Beach response to breakwater layouts of drainage pipe outlets during beach nourishment. *Estuarine*, *Coastal and Shelf Science*, **228**: 106354, https://doi.org/10.1016/i.ecss.2019.106354.

Zhu J, Shi F Y, Cai F et al. 2022. Influences of beach berm height on beach response to storms: a numerical study. *Applied Ocean Research*, **121**: 103090, https://doi.org/10.1016/japor.2022.103090.